doi:10.3772/j.issn.1006-6748.2021.02.008

Magnetic circuit optimization and experimental study of new internally excited automatic balancing①

Li Zhaoju (李兆举)*, Chen Lifang②*,**, Zhou Bo*, Yan Ziwen*, Zhou Shuhua*
(*Key Laboratery of Engine Health Monitoring Control and Networking of Ministry of Education, Beijing University of Chemical Technology, Beijing 100029, P. R. China)
(**Beijing Key Laboratery of Health Monitoring and Self-Recovery for High-End Mechanical Equipment, Beijing University of Chemical Technology, Beijing 100029, P. R. China)

Abstract

Mass imbalance-induced vibration affects the rotating machinery very large, especially the high-speed types. Off-line balancing techniques have been widely developed for rejecting unbalance-induced vibration but do not eliminate unbalanced vibration in the working state. Moreover, multiple start-stops are required in off-line balancing techniques. Therefore, research on an efficient electromagnetically-driven auto-balancer is carried out in the present work, and an internal excitation actuator is designed in this balancer. The electromagnetic characteristics of the two copper coil bobbins in the internal excitation actuator are compared and analyzed. The permanent magnets inside the actuator are simulated and analyzed with different sections of round, rectangular, and elliptical. And the results show that the elliptic type has the largest self-locking force. Finally, the dynamic balance test is performed on a test bench equipped with a designed electromagnetic balancing actuator, and the unbalance vibration is reduced from 130.23 μm to 5.98 μm.

Key words: unbalanced vibration, rotating machinery, automatic balancing actuator, electromagnetic simulation

0 Introduction

In recent years, rotating machinery in the fields of aviation[1] and petrochemicals[2] has developed rapidly with high speed and heavy load capabilities. However, the vibration problems have become more prominent, and the synchronous frequency vibration caused by rotor mass imbalance accounts for more than 70% of the vibration failures of rotating machinery. Off-line balancing techniques have been widely used for dynamic balancing[3]. This method requires shutting down the rotating equipment and performing trial weights, counterweights, and other processes. It requires repeated start-up and shutdown, which is inefficient and costly. Online automatic balancing technology has been born out of this context, and can realize the automatic balancing of rotating machinery without stopping[4].

Online automatic balancing technology can be categorized as either passive or active based on whether the balancing process requires external energy. Passive online balancing works on rotor systems with a working speed higher than the critical speed[5], and has a limited scope of application. Active online automatic balancing technology can be further divided into variable mass-type[6], force-type[7], and mass transfer-type[8] according to the principle of action. The electromagnetic automatic balancing actuator is a typical mass transfer-type online automatic balancing device[9]. The device has two built-in weight plates, and with the help of an electromagnetic driving force, it conducts strategic stepping, synthesizes the counterweight vector, and stabilizes at the counterweight position under the action of a self-locking force, ultimately achieving the online automatic balancing of the rotor system. Since the end of the 20th century, many research institutions and scholars have conducted research on electromagnetically-driven automatic balancing devices. Achievements have been made in structural design[10-11], control algorithms[12-13], and vibration signal acquisition[14], and mature products[15-16] have been developed. However, most of the existing electromagnetic balancing actuators adopt the structural design of a weight plate inside the driving coil. As a result, the radius of the counter-

① Supported by the National Natural Suience Foundation of China (No. 51775030, 91860126).
② To whom correspondence should be addressed. E-mail: chenlf@mail.buct.edu.cn
Received on Mar. 23, 2020

weight is small, which affects the balancing ability of the electromagnetic balancer.

In view of these problems, this paper proposes a new type of internally excited electromagnetic balancing actuator with a counterweight disk outside the excitation coil. Its electromagnetic characteristics are simulated and analyzed, and test verification is conducted. The results demonstrate that the automatic balancing actuator can greatly reduce the vibration value.

1 Electromagnetic automatic balancing actuator

1.1 Overview of electromagnetic balancing actuator structure

As an actuator of the automatic balancing system, the electromagnetic balancing actuator is a key component that determines the success of the entire system. The core components of the electromagnetic balancing actuator are two counterweight disks on which counterweights are fixed. When the copper coil receives a pulse current excitation, the counterweight disks are stepped, and the angle between the two counterweights is changed. A certain compensation vector is synthesized to realize the online automatic balancing of the rotor system. As illustrated in Fig. 1(a), in the conventional externally excited electromagnetic balancing actuator, two counterweight disks are respectively installed inside the excitation coil, and each works independently. This design has the advantage of the balancing actuator being easy to remove, but the structure limits the radius of the counterweight. The proposed internally excited electromagnetic balancing actuator is illustrated in Fig. 1(b). The counterweight disk is designed outside the coil and is connected to the rotor by bearings and external support plates. The two counterweight discs can not only keep rotating synchronously with the rotor (permanent magnetic self-locking state), but also perform directional positioning movement relative to the rotor (electromagnetic driving state). When performing online dynamic balancing, the main controller sends pulse currents to the respective coils corresponding to the weight plate so that the coil frame and the magnetic plate generate external magnetic fields. Under the action of the force of the magnetic field, the permanent magnet drives the weight plate to perform a step motion. Throughout the process, the hall sensor can monitor the positions of the two counterweights in real time.

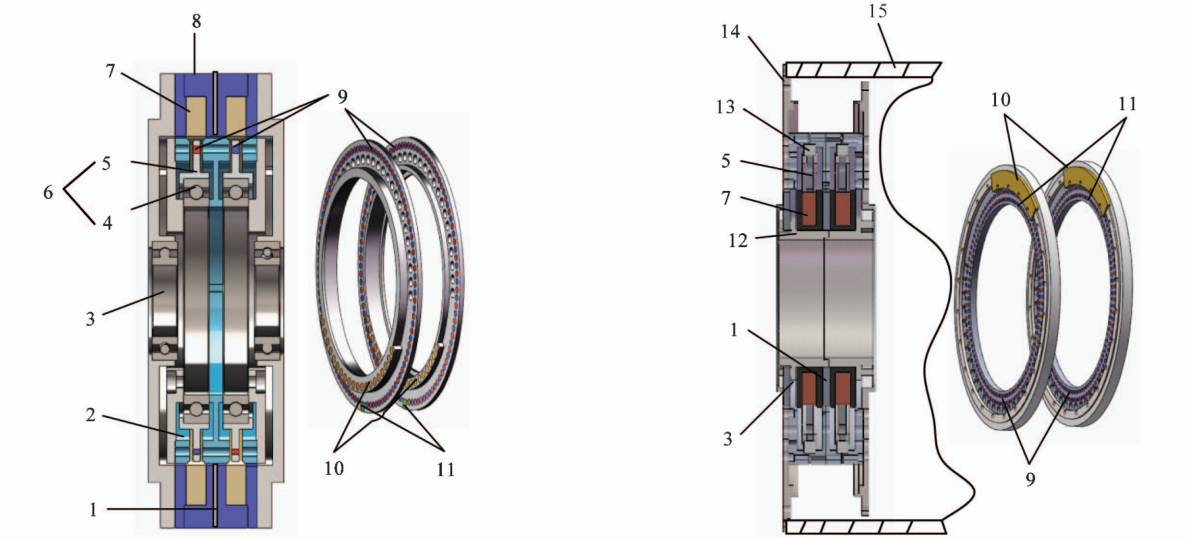

(a) The externally excited electromagnetic balancing actuator (b) The internally excited electromagnetic balancing actuator

1-Magnetic separation plate; 2- Magnetic plate with holes; 3- Static ring bearing; 4- Counterweight disc bearing; 5- Counterweight disc; 6- Ring; 7- Copper coils; 8- Coil bobbin; 9- Permanent magnets; 10- Counterweight; 11- Locate magnet; 12- Static ring; 13- External support bearing; 14- External support plate; 15- Rotor

Fig. 1 Structures of the electromagnetic balancing actuator

1.2 Principle of permanent magnet self-locking for weight plate

The structure that uses the permanent magnet to realize the position locking function of the weight plate is called the permanent magnet self-locking structure. It includes a weight plate, a permanent magnet, and magnetized plates on both sides of the weight plate. When there is no external magnetic field, the entire structure forms a closed permanent magnet magnetic circuit. The permanent magnet is the excitation source of the magnetic circuit, and the magnetic plates on both sides and the air gap serve as paths. In this pa-

per, the magnetic circuit of a self-locking permanent magnet is a series magnetic circuit with an air gap, in which the total magnetic resistance R_m is the sum of the magnetic resistance R_{m0} of the air gap and the magnetic resistance R_{m1} of the magnetic plate. Based on this principle, the magnetic resistance is calculated as

$$R_m = R_{m0} + R_{m1} = \frac{l_0}{\mu_0 S} + \frac{l_1}{\mu_1 S} \quad (1)$$

where l is the magnetic plate length, l_0 is the air gap length, μ_0 is the air permeability, μ_1 is the magnetic plate permeability, S is the effective area of the permanent magnet.

Fig. 2 is a schematic diagram showing a positional relationship between a weight plate and a magnetic plate in a self-locking state. The permanent magnets are alternately installed in the directions of the N and S poles. To further explain the principle of permanent magnet self-locking, a sectional view along the *P-P* circumferential direction in Fig. 2 is illustrated in Fig. 3.

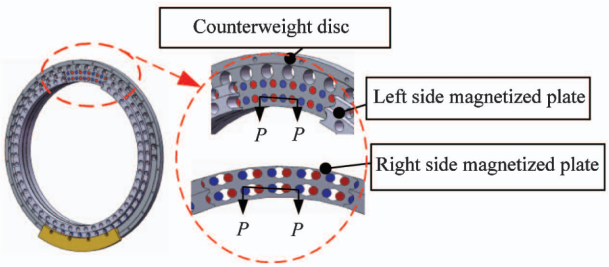

Fig. 2 Schematic diagram of the positional relationship between the weight plate and magnetized plate

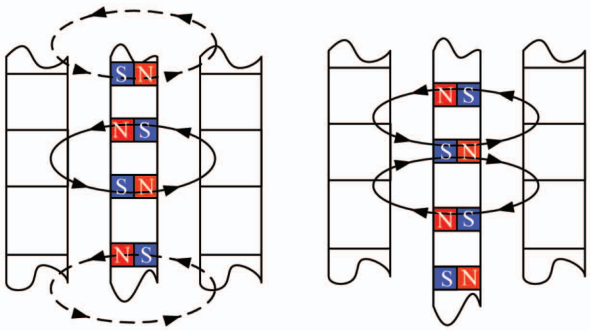

Fig. 3 Schematic diagram of permanent magnet self-locking

1.3 Counterweight drive principle

When a new imbalance occurs in the rotor system, the two counterweight disks need to be stepped into a counterweight vector. A pulse current is sent to the electromagnetic balancing actuator to form an external magnetic field. The magnetic plate is subjected to this magnetic field and exhibits N-pole and S-pole magnetic characteristics at both ends, as shown in Fig. 4.

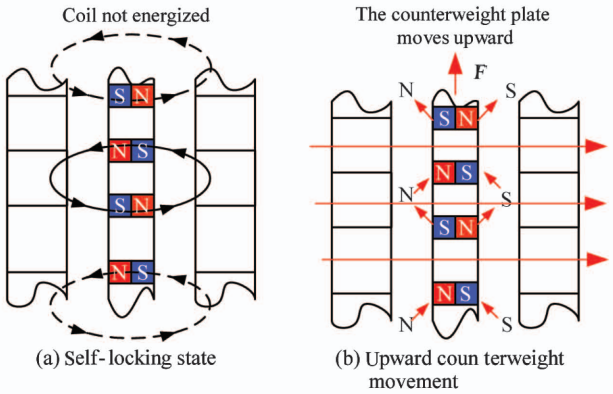

Fig. 4 Principle of electromagnetic driving

Fig. 4 (a) depicts the self-locking state. In the state in which there is no coil excitation, a closed magnetic field is formed by the permanent magnet and the perforated magnetization plate. It is ensured that the weight plate is in a self-locking state. When the rotor system moves at a constant speed, the self-locking force allows the weight plate and the rotor to rotate synchronously.

Fig. 4(b) displays the upward movement of the weight plate. When a mass imbalance vibration occurs in the rotor system, a weight plate is required to perform weight balancing. The coil is energized with a pulsed direct current to magnetize the surface of the magnetic plate to generate controllable N and S poles. According to the principle of attracting the opposite poles of a magnet and repelling the same poles, the permanent magnet generates movement force *F*. The weight plate is further driven to perform a stepping motion relative to the rotor. If direct currents in different directions are alternately supplied to the coil, the counterweight disc will continuously move in one direction.

2 Internally excited structure optimization

The reasonable structural design of the electromagnetic balancing actuator can not only meet the actual installation requirements, but also enables the electromagnetic balancing actuator to obtain the best electromagnetic performance. Therefore, this section focuses on the structure of the electromagnetic balancing actuator, and Maxwell software was used for modeling and simulation. Static magnetic circuit analysis was performed for the magnetic field line closure situation and magnetic induction strength to obtain the best structural design solution.

2.1 Coil bobbin magnetic circuit analysis

2.1.1 Coil bobbin static magnetic field analysis

A two-dimensional analysis model along the verti-

cal plane of the vertical electromagnetic balancing actuator was established, as shown in Fig. 2. The model consists of two sets of independent permanent magnets, side magnetic plates, intermediate magnetic plates, and a coil bobbin. The coil bobbin has two kinds of structures. Fig. 5(a) illustrates an integrated structure (W-shaped structure), Fig. 5(b) illustrates a grouped structure (U-shaped structure). To ensure the quality and efficiency of the grid simulation calculation, the chamfers and shaft shoulders are ignored, the air domain is applied, and the balloon boundary conditions are added to simulate infinite boundary conditions. Permanent magnets are fitted in the counterweight pan. The weight plate is made of aluminum with low magnetic permeability, so the model analysis only considers permanent magnets. The side magnetic plate, the middle magnetic plate, and the coil bobbin are all made of pure iron. Analysis path 1 is established with the starting point as the origin of the relative coordinates.

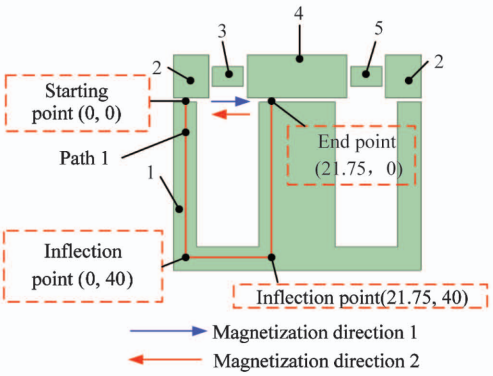

(a) W-shaped structure

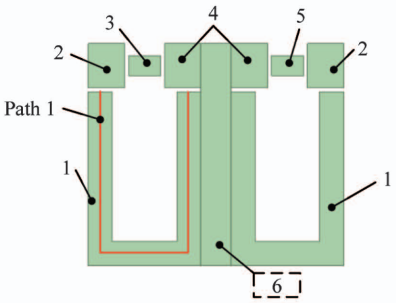

(b) U-shaped structure

1-Coil bobbin (pure iron material); 2-Side magnetic plate (pure iron material); 3-Permanent magnet (counterweight plate 1); 4-Intermediate magnetic plate (pure iron material); 5-Permanent magnet (counterweight plate 2); 6-Medium interval magnetic plate (aluminum material)

Fig. 5 Coil bobbin

Because the two counterweight disks work independently, there are two cases of the magnetization direction of the two sets of permanent magnets, namely the magnetization directions of the two are the same or opposite. Magnetic field lines and magnetic induction intensity maps of the two structures for these cases are presented in Fig. 6 and Fig. 7.

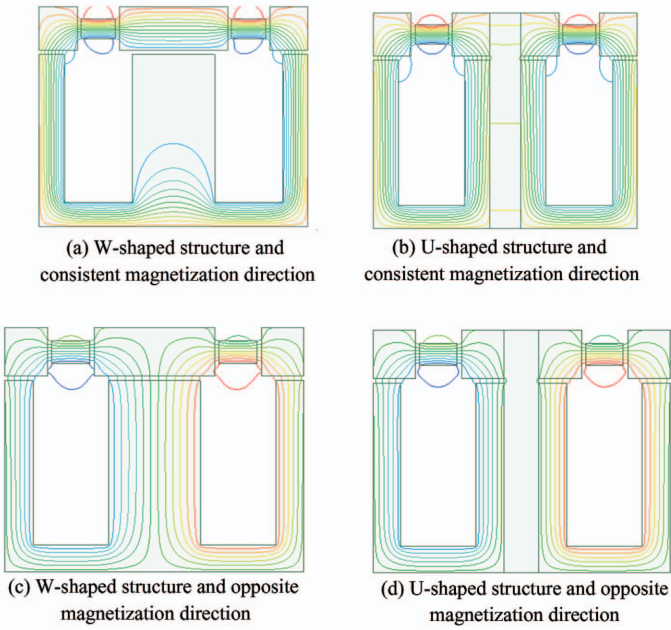

(a) W-shaped structure and consistent magnetization direction

(b) U-shaped structure and consistent magnetization direction

(c) W-shaped structure and opposite magnetization direction

(d) U-shaped structure and opposite magnetization direction

Fig. 6 Magnetic field lines

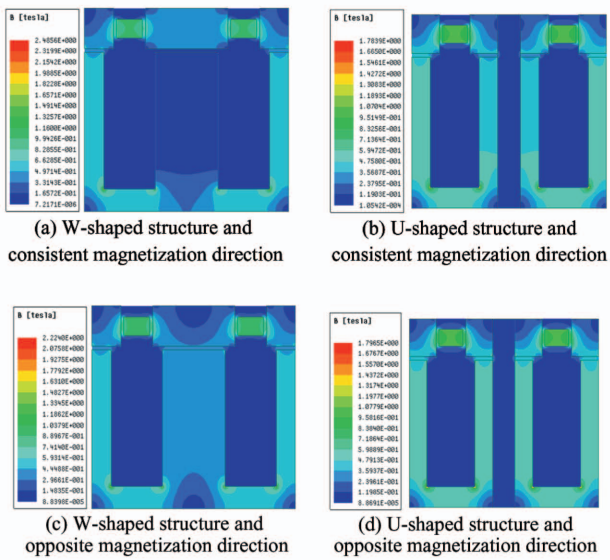

(a) W-shaped structure and consistent magnetization direction

(b) U-shaped structure and consistent magnetization direction

(c) W-shaped structure and opposite magnetization direction

(d) U-shaped structure and opposite magnetization direction

Fig. 7 Magnetic induction intensity map

It is evident from Fig. 6(a) that when the magnetization directions of the two magnets of the W-shaped structure are the same, the magnetic field lines are closed along the outermost periphery of the model, and no magnetic field lines appear in the middle part of the coil frame. As is clear from Fig. 7(a), the magnetic induction intensity distribution in this part is weak. Fig. 6(c) shows that when the magnetization direction is opposite, the magnetic field lines can be closed independently. When the magnetization directions are the same or opposite, the magnetic field lines of the

U-shaped bobbin can be closed, and the magnetic intensity distribution along the coil frame is uniform. Further, a magnetic intensity distribution map of path 1 is presented in Fig. 8.

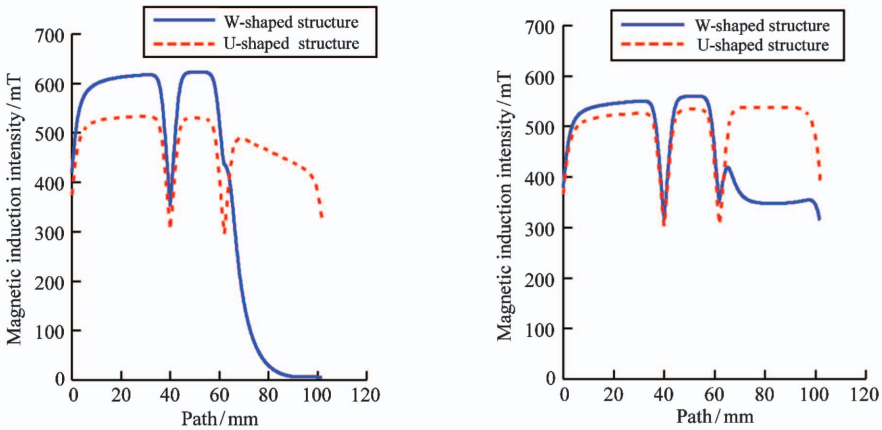

(a) Consistent magnetization direction (b) Oposite magnetization direction

Fig. 8 Magnetic induction along path 1

It can be seen from Fig. 8(a) that when the magnetization directions are the same, the magnetic induction intensity of the W-shaped structure is slightly greater than that of the U-shaped structure at the beginning stage of path 1. However, the magnetic intensity of the W-shaped structure rapidly decays to nearly zero in the later period. The U-shaped structure maintains a relatively stable magnetic induction. When the magnetization direction is opposite, the magnetic induction intensity of the W-shaped structure at the beginning of path 1 is slightly greater than that of the U-shaped structure. However, the magnetic induction intensity of the W-shaped structure in the later period is greatly attenuated. The U-shaped structure maintains a relatively stable magnetic induction. Overall, the uniformity of the magnetic induction of path 1 of the U-shaped structure is better than that of the W-shaped structure.

2.1.2 Coil bobbin startup magnetic field analysis

In addition to considering the magnetic induction distribution of the static magnetic field, the magnetic field distribution of the coil current excitation should also be analyzed. As shown in Fig. 9, a current of 500 A was applied to the copper coil in the bobbin, and the current also existed in two directions. The role of the current is to magnetize the side and middle magnetics plate so that they have N pole and S pole. The magnetic field lines are emitted from the N pole and returned to the S pole, forming the magnetization direction represented by the dotted line in the figure. It is evident from Fig. 7 that when the magnetization directions of the two magnets are the same, the magnetic field intensity distribution in the middle of the W-shaped bobbin is weak. Therefore, this section analyzes the electromagnetic distribution characteristics of the two coil bobbin structures when the magnetization directions are the same. When the magnetization direction of the two magnets is 1, according to Ampere's rule, it is known that the current direction needs to be in an inward vertical plane, which is the working condition 1. At this time, the closed magnetic field of the model is formed, as illustrated in Fig. 9(a) and Fig. 9(b). When the magnetization direction of the two magnets is 2, the direction of the current needs to be directed outward from the vertical plane, which is the working condition 2, as illustrated in Fig. 9(c) and Fig. 9(d). In these two working conditions, the magnet

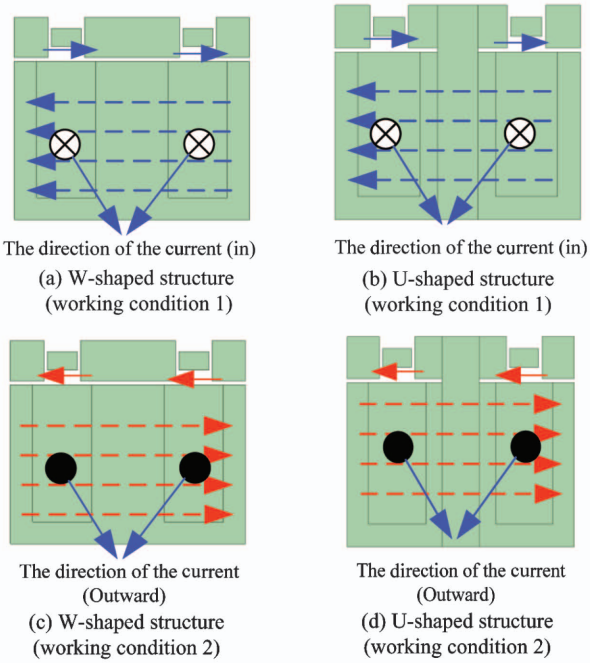

(a) W-shaped structure (working condition 1)
(b) U-shaped structure (working condition 1)
(c) W-shaped structure (working condition 2)
(d) U-shaped structure (working condition 2)

Fig. 9 Start magnetic field structure

is attracted. If the above four conditions are not met, the magnetic field will be closed along other paths, and the magnet will be repelled. In the same way, the magnetic force line diagram and magnetic induction cloud diagram for the four cases obtained by analysis are presented in Fig. 10 and Fig. 11.

It can be seen from Fig. 10(a) and Fig. 10(c) that the W-shaped structure is closed along the periphery under working conditions 1 and 2, and the middle part of the coil bobbin is less distributed, while the magnetic lines of the U-shaped structure are closed independently and distributed uniformly. Fig. 11(a) and Fig. 11(c) show that the magnetic induction intensity distribution in the middle of the W-shaped bobbin is relatively weak, while the magnetic induction intensity of the U-shaped structure is uniformly distributed along the stent coil holder. Magnetic induction intensity distribution diagrams of path 1 under working conditions 1 and 2 are presented in Fig. 12.

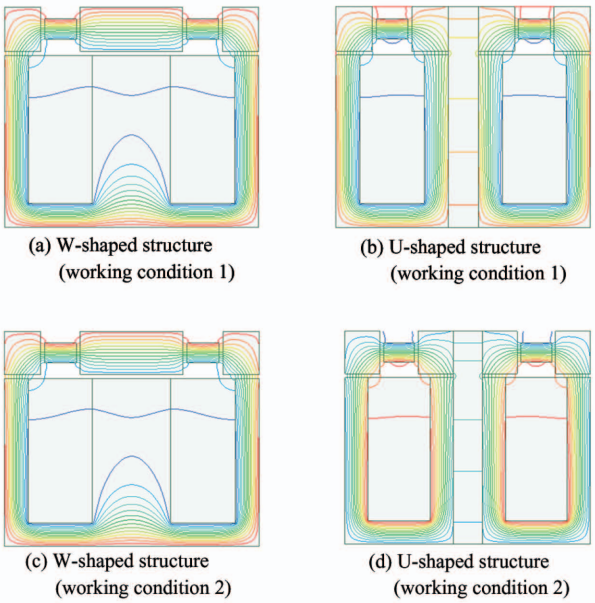

Fig. 10 Magnetic line diagram

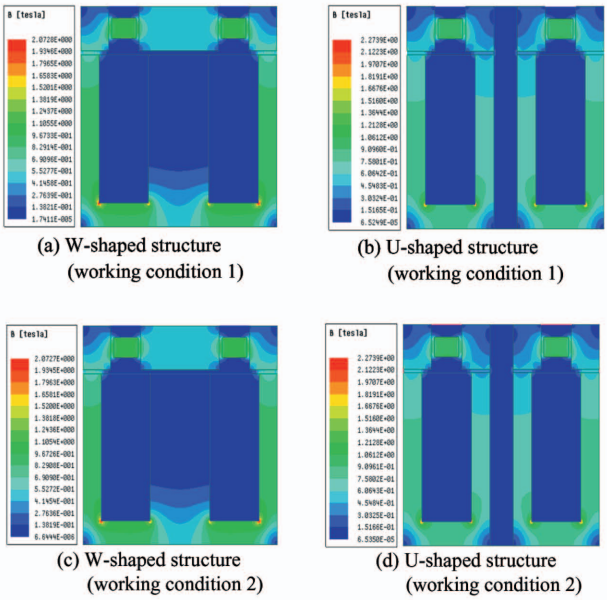

Fig. 11 Magnetic intensity distribution

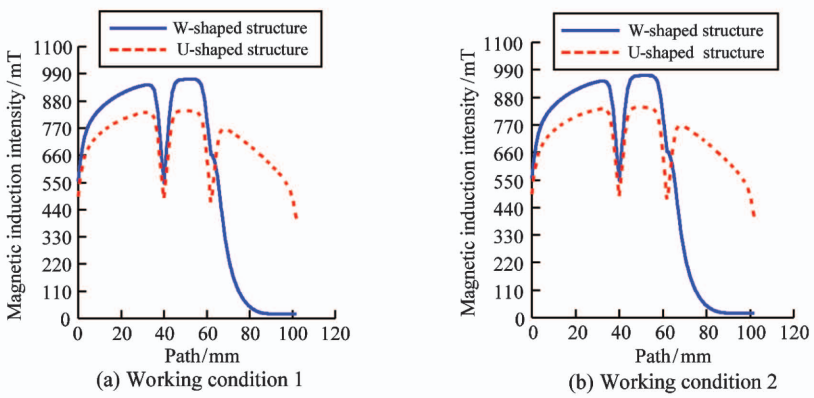

Fig. 12 Distribution of magnetic induction along the path 1

It can be discerned from Fig. 12 that under the two working conditions, the magnetic induction intensity distribution of the U-shaped structure along the entire coil bobbin path is generally above 330 mT. However, the magnetic flux density of the second half of path 1 of the W-shaped structure decreases sharply. Therefore, the second half of the W-shaped bobbin path is not fully utilized.

2.2 Effect of magnetic source on electromagnetic characteristics of U-shaped structure

An electromagnetic analysis of U-shaped structures is presented in this section. Based on the path 1 designed previously, a side magnetic plate path 2 and an air gap path 3 are added. The starting points of the three paths are the relative coordinate origins of each path, as illustrated in Fig. 13.

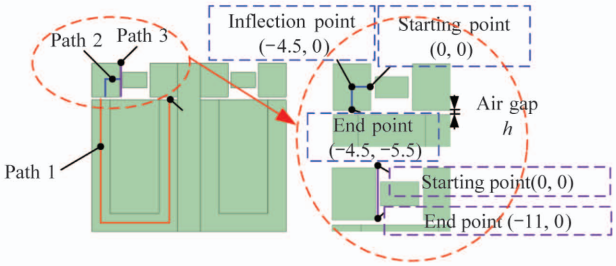

Fig. 13 Schematic diagram of paths 2 and 3

An analysis was performed to obtain distribution maps of the magnetic induction intensities along the three paths at current excitations of 250, 500, 750, and 1000 A. It is clear from Fig. 14(a) that along the path of the coil bobbin, as the current increases, the magnetic induction intensity also increases. The magnetic induction intensity distribution of the entire 1000 A path is located above other currents, with a maximum of 1152.32 mT. It can be seen from Fig. 14(b) that the magnetic induction intensities at the start and end points of path 2 of the side magnetic plate are generally greater than those at other positions. Under the same 1000 A current excitation, the magnetic induction intensity of the entire path is generally greater than that under other currents, with a maximum value of 915.06 mT. Fig. 14(c) shows that the magnetic flux densities at the start and end points of path 3 of the air gap are small. The distribution of magnetic induction intensity is the largest under the current of 1000 A, reaching 898.64 mT. The structure current is 250 – 1000 A, and the magnetic induction intensity has not reached saturation. The driving current can be adjusted according to the actual working conditions.

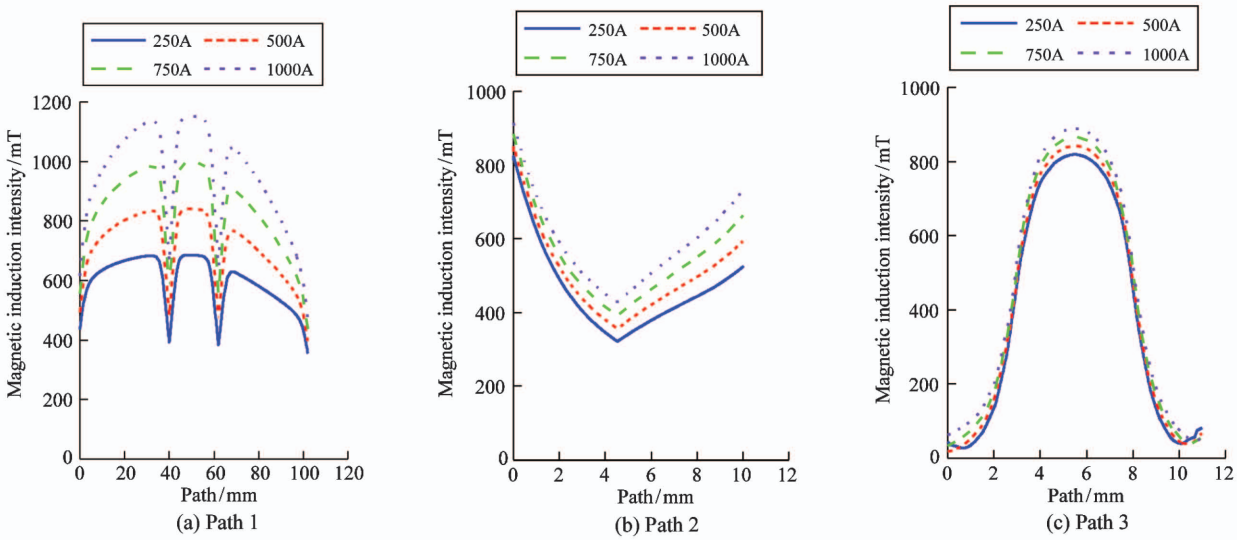

Fig. 14 Distribution of magnetic induction intensity under different currents

3 Optimization of self-locking magnetic circuit of weight plate

3.1 Selection of different permanent magnetic materials

The mechanism of the permanent magnet self-locking magnetic field presented in Fig. 3(a) is to rely on the principle of the spontaneous magnetization of permanent magnetic materials to form a closed magnetic circuit. An analysis model presented in Fig. 15 is established, and the gap δ and path 4 between the permanent magnet and the magnetic plate are defined. The area between 2.5 mm and 5 mm in path 4 is the part where the permanent magnet and the magnetic plate are directly opposite, and this part is collectively called the main working air gap section. The permanent magnet is 5 mm in diameter and 8 mm in length. Different types of permanent magnets were used for analysis, as listed in Table 1. The magnetic induction intensity distribution diagrams of the four cases are presented in Fig. 16.

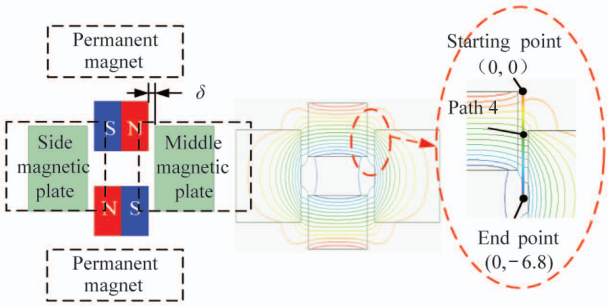

Fig. 15 Schematic diagram of self-locking magnetic circuit

Table 1 Permanent magnet parameters

Material type	Grade	Coercive force/kA/m	Relative permeability
NdFeB	NdFe35	890	1.10
SmCo permanent magnet	SmCo24	756	1.06
Rare earth cobalt permanent magnet	XG112/96	520	B-H curve
Ferrite permanent magnet	Y10T	140	B-H curve

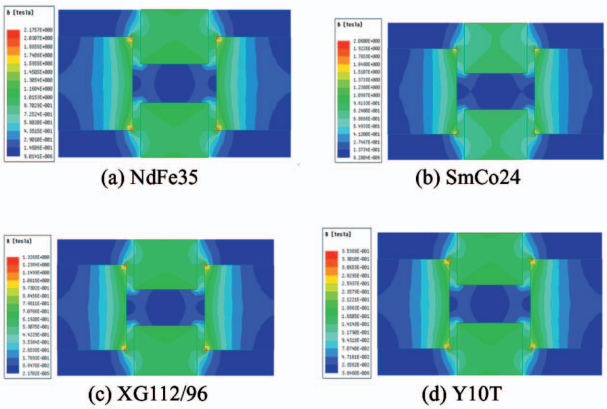

Fig. 16 Magnetic induction intensity of different permanent magnets

Fig. 16 shows that the magnetic induction distributions of the four types of permanent magnets are similar. Among them, the self-locking structure of the NdFe35 permanent magnet was found to have the largest magnetic induction intensity of 2.17 T. To quantitatively analyze the distributions of the four types of magnetic induction intensity, a magnetic induction intensity distribution map along path 4 is presented in Fig. 17(a). Additionally, the magnetic induction intensity was integrated along the path to obtain the A value, as given by Eq. (2). Four A values were calculated, as shown in Fig. 17(b).

$$A = \int_{l_4} B\mathrm{d}l \tag{2}$$

where B is magnetic induction intensity, l_4 is path 4, A is the integration of magnetic induction intensity.

It can be determined from Fig. 17 that under the same structural conditions, the self-locking structure of the NdFe35 permanent magnet is superior, and has a large magnetic induction strength of up to 989.93 mT. The integral along the path is also the largest, with a value of 3.77×10^{-3} Wb/m. The magnetic induction intensity distribution of the working air gap section is between 508.39 and 989.93 mT. In summary, the self-locking structure that uses NdFe35 is the most efficient.

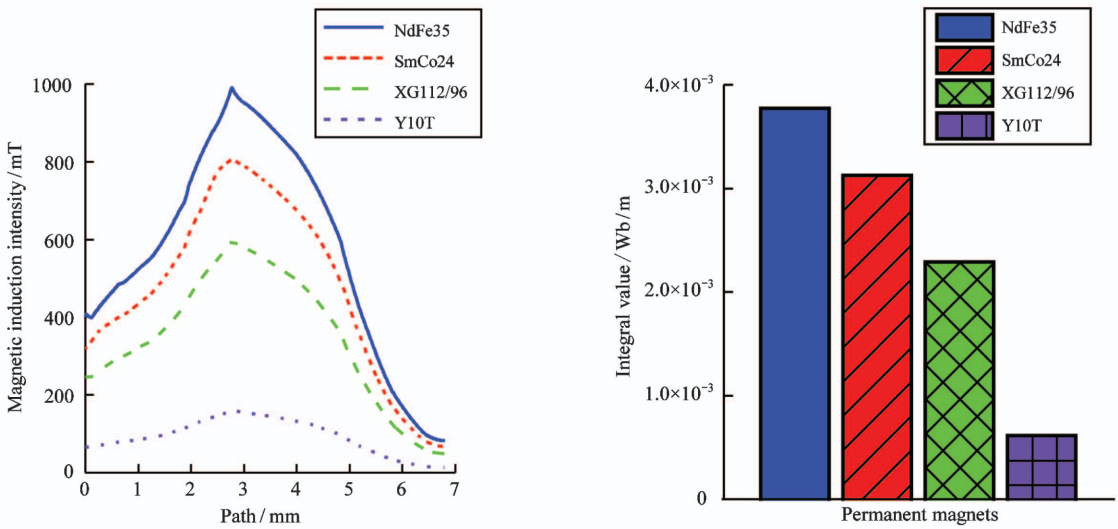

Fig. 17 Distribution of electromagnetic characteristics of different permanent magnets along path 4

3.2 Influence of different permanent magnet shapes on magnetic field characteristics

When the weight plate performs a continuous stepping motion, shaking and even overshooting may sometimes occur when reaching the self-locking position. At this time, the transmission of a pulse excitation is accompanied by the unsteady stepping of the weight plate by two positions. This situation will cause the active balancing system to fail to actively suppress the vibration, primarily because the self-locking force of the counterweight disk is not sufficiently stable. To this end, three different shapes of permanent magnets,

namely with circular end faces, rectangular end faces, and elliptical end faces, are proposed in this section from the perspective of structural design, as presented in Fig. 18. The simulation analysis of the self-locking force is found to change in the three cases.

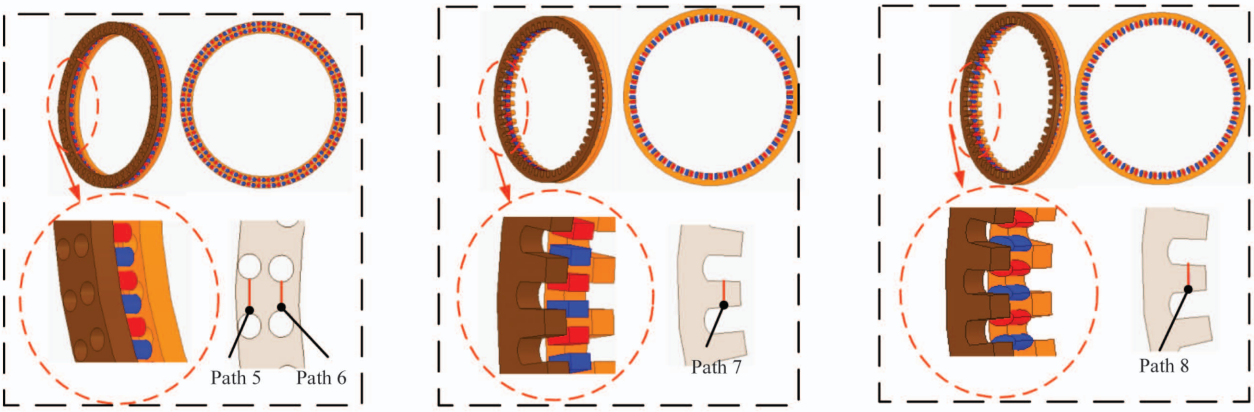

(a) Round end face (b) Rectangular end face (c) Oval end face

Fig. 18 Permanent magnets of different shapes

The total areas of the three types of end faces of the magnets are basically the same. Additionally, the magnetic plate uses a ring with an outer diameter of 272 mm and an inner diameter of 117 mm, and the end surface areas removed by the ring are basically the same. The first structure is a round end face magnet. To improve the self-locking force, a double-row magnet arrangement is used. The diameter of the magnet is 5 mm. The total end face area of 200 magnets is 3926.99 mm^2. The total surface area removed is 4133.16 mm^2. The second type of rectangular magnet has an end area of 3927.72 mm^2, and the magnetic plate is opened into a rectangular through-hole. The total removed area is 4136.54 mm^2. The third type of elliptical magnet has a total end area of 3939.00 mm^2 and a removed area of the magnetic plate of 4136.54 mm^2. Paths 5 and 6 are defined between the two columns of vias in Structure 1, path 7 is defined in Structure 2, and path 8 is defined in Structure 3. The calculated self-locking forces are reported in Table 2.

Table 2 reveals that the self-locking force of Structure 1 is 14.39 N · m, that of Structure 2 is 19.28 N · m, and that of Structure 3 is 21.86 N · m; thus, under the same structural conditions, the self-locking force of Structure 3 is the largest. In addition, the magnetic intensity distribution curves of paths 5, 6, 7, and 8 are presented in Fig. 19.

As presented in Fig. 19(a), the magnetic induction intensity of the magnetic plate of Structure 1 has a large range, and decreases sharply in the middle. The lowest magnetic induction intensity of path 5 is 36.60 mT, and that of path 6 is 11.14 mT; therefore, this structure has an uneven magnetic induction intensity distribution. As presented in Fig. 19(b) and Fig. 19(c), the magnetic induction intensity distribution of path 7 is between 802.91 and 1893.91 mT, and that of path 8 is between 795.76 and 2199.40 mT. Structures 2 and 3 therefore have a more uniform magnetic induction intensity in the middle than Structure 1 does.

In summation, the self-locking force of the elliptical magnet is the largest, and the corresponding magnetic induction intensity distributions of Structures 2 and 3 are uniform. However, it cannot be ignored that the circular magnet is a standard component on the market, and its cost is low; in contrast, rectangular and oval magnets are non-standard pieces.

Table 2 Permanent magnet parameters

Parameter	Structure 1	Structure 2	Structure 3
Magnet end shape	Round face	Rectangular end face	Oval face
Total surface area of magnet/mm^2	3926.87	3927.72	3939.00
Removed area of magnetic plate/mm^2	4133.16	4136.54	4136.54
Self-locking force/N · m	14.39	19.28	21.86

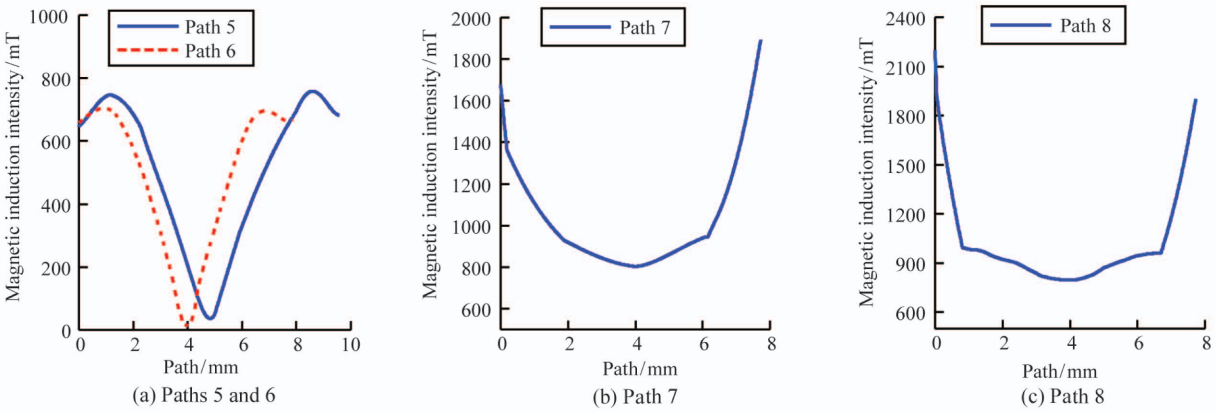

Fig. 19 Magnetic induction of different paths

4 Experimental research

4.1 Automatic balancing test bench

A simulated electromagnetically-driven automatic balancing test bench was constructed, as illustrated in Fig. 20. The cantilever end of the rotor was equipped with an internally excited balancing actuator (with a balance capacity of 60 g · m). The balancing actuator was built into the engine rotor . An eddy current displacement sensor was installed in the vertical direction of the rotor. The Hall signal of the counterweight disk and the vibration signal of the rotor were collected by an nDAQ9184 acquisition system produced by NI Corporation, and the signals were programmed and processed in real time using LabVIEW software. Additionally, an integrated electromagnetically-driven main controller was designed to achieve the electromagnetically-driven automatic balancing of the two counterweight disks in any direction and position. The control signal was output through the PLC high-speed pulse output port, and the coils of the two counterweight diskswere pulsed to drive the counterweight disks to step and generate the required counterweight vector.

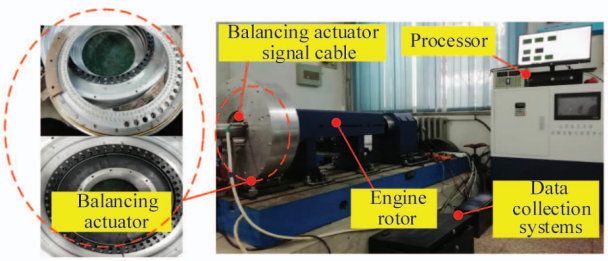

Fig. 20 Automatic balancing test bench

4.2 Automatic balancing test

This section reports the results of the automatic balancing test verification. The test bench rotor was rotated at a constant speed of 1020 r/min, and the vertical amplitude was used as the automatic balancing input signal. The calculation of the number of steps of the counterweight plate was performed based on the influence coefficient method. The controller triggered the movement of the counterweight plate. An automatic balancing test of the rotor with unbalanced vibration failure was performed. It can be seen from Fig. 21 that the amplitude before the automatic balancing test was 130.23 μm. After 25 s of automatic balancing, the amplitude was reduced to 5.98 μm, the amplitude reduction value was 124.25 μm, and the vibration reduction ratio was 95.41%. The level of rotor vibration was significantly reduced. Additionally, the relationship between the angle values of the two counterweight discs after the automatic balancing test is plotted in Fig. 22. After the automatic balancing test, weight plate 1 was maintained at 118.8 °, and weight plate 2 was maintained at 21.6 °. The device can therefore achieve stable self-locking without angular offset.

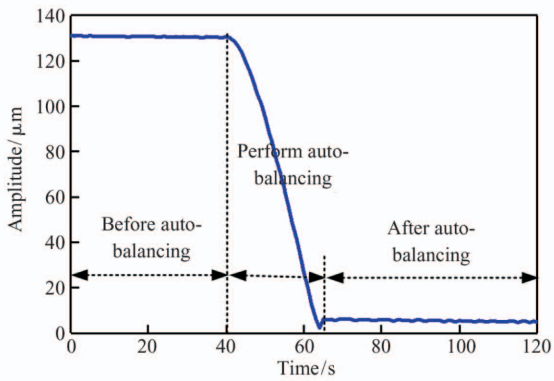

Fig. 21 Automatic balancing test

5 Conclusions

This paper introduces an internally excited electromagnetic balancing actuator, and analyzes two types of coil bobbin structures of the balancing actuator. It is

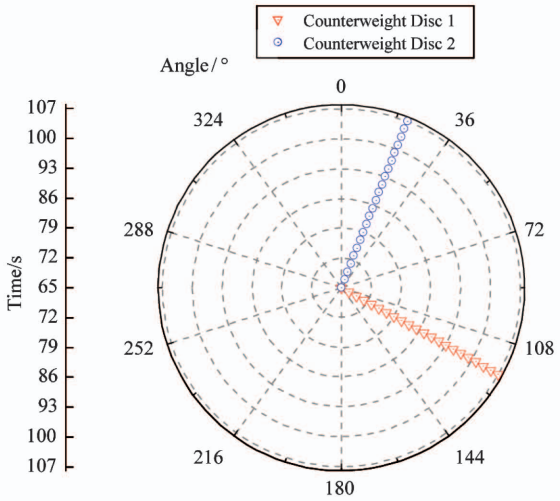

Fig. 22 Counterweight angles

found that the U-shaped coil bobbin has uniform distributions of the magnetic lines of force and magnetic induction as compared to the bobbin of the W-shaped structure. Additionally, the shapes of three permanent magnets are compared and analyzed. It is found that the magnetic induction intensity of the magnetic plate with an oval shape and a corresponding opening had a uniform distribution, and its self-locking force is the largest, reaching 21.86 N · m. Finally, an automatic balancing test study based on the proposed type of internally excited balancing actuator is carried out. The test results demonstrate that the vibration reduction effect is obvious, the amplitude reduction value is 124.25 μm, and the vibration reduction ratio is 95.41%. The balancing actuator can realize stable self-locking.

References

[1] Chen L F, Wang W M, Gao J J. Summary on the development of auto-balancing technology of aero-engine[J]. *Journal of Aerospace Power*, 2019, 34(7): 1530-1541

[2] Liu B B. Key Technology Research on Rotor Stability and Axial Displacement Fault Prevention of Centrifugal Compressor[D]. Beijing: College of Mechanical and Electrical Engineering, Beijing University of Chemical Technology, 2018: 1-3

[3] Chu Z, Huang D, Yang L. Field balancing of vehicle transmission shaft based on the influence coefficient method[J]. *Noise and Vibration Worldwide*, 2018, 49(7-8): 266-271

[4] Zhang S H, Wang Y S, Zhang Z. Online dynamic balance technology for high speed spindle based on gain parameter adaption and scheduling contronl[J]. *Applied Sciences*, 2018, 8(6): 917

[5] Li B Y. Research on Influence of the Trach's Eccentricity on Dynamic Characteristics of Ball-type Automatic Balancer[D]. Changsha: College of Mechanical and Electrical Engineering, Central South University, 2014: 1-5

[6] Pan X, Xie Z, Lu J, et al. Novel liquid transfer active balancing system for hollow rotors of high-speed rotating machinery[J]. *Applied Sciences*, 2019, 9(5): 833

[7] Jiang H, Sun Z Z, Wang D. Dynamic modeling of magnetic bearing-rotor system on moving platform[J]. *Transactions of China Electrotechnical Society*, 2019, 34(23): 4880-4889

[8] Pan X, He X T, Wei K Z, et al. Performance analysis and experimental research of electromagnetic-ring active balancing actuator for hollow rotors of machine tool spindles[J]. *Applied Sciences*, 2019, 9(4): 692

[9] Fan H W, Jing M Q, Liu H. New machine tool motorized spindle integrated with one electromagnetic ring balancer driven by optimal square wave[J]. *Journal of Mechanical Engineering Science*, 2015, 229(8): 1509-1522

[10] Liu F G, Chen L F, Wang W M, et al. Factors influencing the self-locking force of an on-line automatic balancing device[J]. *Journal of Beijing University of Chemical Technology (Natural Science)*, 2016, 43(2): 114-121

[11] Yang T T, Jing M Q, Fang H W, et al. Drive parameter optimization method to improve operation smoothness of electromagnetic balancer[J]. *Electric Machines and Control*, 2015, 19(5): 14-20

[12] Fang H W, Zhi J J, Shi B J, et al. Adaptive rotor balancing algorithm and single-disk rotation test for electromagnetic balancer[J]. *Journal of Xi'an Jiaotong University*, 2018, 52(8): 15-29

[13] Chen L F, Chen Z C, Wang W M, et al. Nonstationary autobalancing control based on adaptive particle swarm optimization[J]. *Journal of Vibration and Shock*, 2018, 37(24): 131-136

[14] Zhu F L. Study on the High Speed Spindle Online Dynamic Balancing Vibration Signals Dealing and Regulation Basing on LabVIEW[D]. Shenyang: College of Mechanical Engineering, Shenyang Jianzhu University, 2019: 2-6

[15] Hofmann C. Active balancing available online. [EB/OL]. https://www.hofmann-global.com/en/products/active-balancing-systems.html: Hofmann Corporation, 2020

[16] Lord C. Propeller balancing available online[EB/OL]. https://www.lord.com/china/products-and-solutions/active-vibration-control/aerospace-and-defense/propeller-balancing.html: Lord Corporation, 2020

Li Zhaoju, born in 1992. He is studying for his M.S. degree in Key Laboratory of Engine Health Monitoring Control and Networking of Ministry of Education of Beijing University of Chemical Technology. He received his B.S. degree in Process Equipment and Control Engineering Department of Shandong University of Science and Technology in 2016. His research interests are automatic balancing technique and vibration control.